Novel Gain of Function Mouse Model of KCNT1-Related Epilepsy

Sarah L. Olguin[1,2], Daniel Davis[3,4]; Ammara Rehman[1,5], Elizabeth Sahagun[1,2]; Payton S. Oswalt[3], Mandar Patil[1,5], Paula D.M. Sullivan[1,5], Bing Zhang[6], **Elizabeth C. Bryda[3,4*], Roy Ben-Shalom[1,5*], Jill L. Silverman[1,2*]**

Affiliations:
[1]MIND Institute, University of California Davis School of Medicine, Sacramento, CA 95817, USA. [2]Department of Psychiatry and Behavioral Sciences, University of California Davis School of Medicine, Sacramento, CA 95817, USA. [3]Veterinary Pathobiology, College of Veterinary Medicine, University of Missouri, Columbia, MO, 65201, USA. [4] MU Animal Modeling Core University of Missouri, Columbia, MO, 65201, USA. [5]Department of Neurology, University of California Davis School of Medicine, Sacramento, CA 95817, USA [6]Division of Biological Sciences, University of Missouri, Columbia, MO 65201, USA.

***Co-Corresponding Authors:**
Jill L. Silverman
MIND Institute and Department of Psychiatry and Behavioral Sciences
4625 2nd Ave Suite 1001A
Sacramento, CA 95817
Phone: 916-734-8531
jsilverman@ucdavis.edu

***Co-Corresponding Authors:**
Elizabeth Bryda, Ph.D.
Department of Veterinary Pathobiology, University of Missouri
4011 Discovery Drive
Columbia, MO 65201
Phone: (573) 882-5504
brydae@missouri.edu

***Co-Corresponding Authors:**
Roy Ben-Shalom
MIND Institute and Department of Neurology
rbenshalom@ucdavis.edu

Keywords: *KCNT1, Epilepsy, epileptic encephalopathy, behavior, seizures, excitability, mouse model, hyperexcitability, epilepsy, channel, potassium, DEE*

Conflict of Interest: The authors declare no conflicts of interest.

Acknowledgements: This work was supported by the MIND Institute's Intellectual and Developmental Disabilities Resource Center NIH P50HD (LA), the NIMH ARTP R01MH117130 (JAG), and Research Council Grant URC-21-027 from the Office of Research, University of

Missouri (ECB). The mouse model was generated by the University of Missouri Animal Modeling Core.

Funding Sources: This work was supported by the MIND Institute's Intellectual and Developmental Disabilities Resource Center P50HD103526 and an MDBR award from the KCNT1 Foundation and the University of Pennsylvania Orphan Disease Center (JLS, SLO), Hartwell Foundation Biomedical Fellowship (JLS; SLO), and Research Council Grant URC-21-027 from the Office of Research, University of Missouri (ECB).

Abstract

KCNT1-related epilepsy is an autosomal dominant neurodevelopmental disorder resulting from *de novo* pathogenic variants in *KCNT1* which encodes a sodium-gated potassium channel. These variants are associated with Epilepsy of Infancy with Migrating Focal Seizures (EIMFS) and Autosomal Dominant Nocturnal Frontal Lobe Epilepsy (ADNFLE). At least 64 human *KCNT1* variants have been reported, the majority are gain-of-function and each has unique electrophysiological and epileptic characteristics. A multi-disciplinary collaboration generated a novel mouse model (C57BL/6-*Kcnt1*^{em1Bryd}) that carries the G269S variant corresponding to the human G288S variant located within the coding region of the channel pore. We characterized network excitability of cultured cortical neurons from all three genotypes, since many *KCNT1* mouse models require homozygosity for seizure detection. *Kcnt1*$^{+/G269S}$ neurons exhibited sustained hyperexcitability and hypersynchronous bursting versus *Kcnt1*$^{+/+}$ controls, while *Kcnt1*$^{G269S/G269S}$ neurons showed early excessive bursting followed by network collapse by 28 days-in-vitro, suggesting excitotoxicity. Therefore, behavioral comparisons were conducted between *Kcnt1*$^{+/G269S}$ and *Kcnt1*$^{+/+}$ mice including developmental milestones, motor and cognitive abilities, respiratory physiology, and seizure susceptibility. *Kcnt1*$^{+/G269S}$ displayed no abnormal gross motor abilities, poor coordination, erratic breathing, and increased apneas, as functional outcome measures. Critically, *Kcnt1*$^{+/G269S}$ were more susceptible to thermal-induced seizures in early life. In summary, these data: (i) provide a novel mouse model of KCNT1-related epilepsy, (ii) provide strong *in vitro* evidence of neuronal hyperexcitability, (iii) illustrate early-life seizures as a functional outcome measure, and (iv) lay the groundwork for future analysis of neural activity *in vivo* and modeling circuit level dynamics *in vitro*, *in vivo*, and *in silico*.

Significance Statement

Gain-of-function mutations in the sodium-gated potassium channel KCNT1 have been linked to pediatric epilepsy of varying severity. The human *KCNT1* variant G288S (G269S in mice) is linked to Autosomal Dominant Nocturnal Frontal Lobe Epilepsy (ADNFLE), Epilepsy of Infancy with Migrating Focal Seizures (EIMFS), and other severe developmental epileptic encephalopathies. There are currently no therapeutics to prevent the progression of *KCNT1*-related epilepsy, therefore, the scientific community requires a novel mouse model that is well characterized, *in vitro* and *in vivo*, to screen and assess targeted therapeutics. Herein, we engineered a novel mouse to assess developmental and adult phenotypes resulting from the G288S/G269S variant, *in vitro* and *in vivo*, to advance translation toward therapeutic testing for individuals with *KCNT1*-related epilepsy.

Introduction

Genetic studies have revealed about one-third of neurodevelopmental disorders (NDDs) are associated with gene mutations affecting neuronal ion channels, emphasizing their importance in pathology (Noebels 2017; Daghsni et al. 2018; Satterstrom et al. 2020). Understanding how these mutations alter channel kinetics makes *in vivo* experimental models essential (Sanders et al. 2018; Smith and Walsh 2020; Niemi et al. 2018; Sigg 2014; Sakmann and Neher 1984; Harris 2021; Spmouset et al. 2019; Almog et al. 2021). The *KCNT1* gene encodes a sodium activated potassium (K_{Na+}) channel, which regulates neuronal excitability by affecting resting membrane potential and hyperpolarization following action potentials. The electrophysiological properties of *KCNT1* variants differ significantly, contributing to distinct epileptic syndromes including Epilepsy of Infancy with Migrating Focal Seizures (EIMFS), Autosomal Dominant Nocturnal Frontal Lobe Epilepsy (ADNFLE), West syndrome, and Ohtahara syndromes (Hinckley et al., 2023; Rychkov et al., 2022). Importantly, *KCNT1*-related epilepsy often begins early in life and is treatment resistant. Bonardi et al. (2021) identified 64 *KCNT1* mutations in 248 individuals (Bonardi et al., 2021), however, few *in vivo* mouse models exist.

Homozygous *Kcnt1*$^{-/-}$ mice exhibit poor motor ability in the open field and impaired motor learning, however, seizure related metrics were similar to WT (Quraishi et al., 2019). A model of the R455H variant (human R474H) resulted in increased potassium currents in glutamatergic neurons (Lim et al., 2016) and suppression of inhibitory neuron firing (Wu et al., 2024). This occurs when dysfunctional channels activate rapidly in response to sodium influx during action potential upstroke which can promote hyperexcitability by limiting sodium channel inactivation. Video-EEG of *Kcnt1*$^{+/R455H}$ mice revealed persistent interictal spikes, spontaneous seizures, and reduced pentylenetetrazol (PTZ)-induced seizure threshold (60mg/kg; Quraishi et al., 2019). The

homozygous P924L variant causes frequent debilitating seizures and developmental compromise (Burbano et al., 2022).

The experimental model Y777H (human Y796H) illustrated sleep disturbance due to elevated seizure bouts and length (Wang et al., 2025), both *Kcnt1*$^{+/Y777H}$ and *Kcnt1*$^{Y777H/Y777H}$ were susceptible to kainic acid (KA) and pentylenetetrazol (PTZ)-induced seizures (Shore et al., 2020). Conditional expression of Y777H had no effect on glutamatergic neurons but, increased subthreshold K_{Na+} current in inhibitory neurons (Shore et al., 2024). This cell type-specific modulation creates network imbalance, with certain inhibitory neurons becoming functionally silenced while excitatory neurotransmission remains intact or enhanced (Yang et al., 2024; Rychkov et al., 2022). The loss-of-function (LOF) variant, P932I, is associated with severe early infantile epileptic encephalopathy (EE) and abnormal myelination (Vanderver et al., 2014).

As each *KCNT1* variant affects channel kinetics differently—through distinct alterations in activation thresholds, open probability, and current amplitude (Xu et al., 2022; Rychkov et al., 2022)—their impact on neuronal excitability and seizure susceptibility likely varies considerably across mutation and neuronal subtype, in addition to background strain of the *in vivo* rodent model, (Yang and Frankel, 2004; Miller et al., 2014; Copping et al., 2019; Sukoff Rizzo et al., 2020), adding complexity to understanding circuit-level dysfunction in *KCNT1*-related epilepsies.

D*rosophila melanogaster* lacks a *KCNT1* ortholog, allowing for introduction of the human *KCNT1* gene. While, the WT *hKCNT1* gene showed no phenotype, expression of GOF human variants exhibited seizure rates of 41% (G288S), 48% (R398Q), and 38% (R928C), respectively (Ehaideb et al., 2018; Zhang et al., 2021). Zhang's laboratory illustrates that *hKCNT1* G288S and R928C mutations result in increased K+ conductance, impaired larvae locomotion, hyperpolarized resting potential, and lower muscle resistance (Ehaideb et al., 2018). Consistent

with Zhang, expression of the G288S variant in HEK cells exhibits: (i) a 21-fold increase in K_{Na+} current amplitude; (ii) a ~20% increase in open probability; (iii) a hyperpolarizing shift in activation threshold, reducing voltage sensitivity (Xu et al., 2022); and (iv) minimal impact on time constants/kinetics (Rychkov et al., 2022). This data encouraged the generation of the *Kcnt1* GOF G288S (G269S in mice) experimental model, termed B6-*Kcnt1*^{em1Bryd}. Subsequently, we performed a tailored characterization to define neuronal excitability *in vitro* electrophysiological characteristics and functional outcomes *in vivo,* relevant to *KCNT1*-related epilepsy.

Materials and Methods.

Generation of the G288S Variant (G269S Mouse Model): All experimental procedures were performed in accordance with the National Institutes of Health (NIH) Guide for the Care and Use of Laboratory Animals and approved by the Institutional Animal Care and Use Committees (IACUC) at the University of Missouri and University of California, Davis School of Medicine. The novel *Kcnt1* mutant mouse model was generated by the MU Animal Modeling Core (Columbia, MO) using a standard knockin method involving CRISPR/Cas9 genome editing. The strategy for generating the *Kcnt1* exon 11 codon change was to replace the wild-type mouse *Kcnt1* gene codon GGG with AGC creating a missense mutation. Glycine (G) is replaced by serine (S) at amino acid position 269 in the mouse *Kcnt1* protein which mimics the G288S human variant. C57BL/6J (stock #000664) animals were purchased from the Jackson Laboratory (Bar Harbor, ME). Superovulated females (4-5 weeks of age) were mated to stud males (~10 weeks of age) overnight and zygotes were collected the following morning. sgRNAs were ordered as chemically modified synthetic sgRNAs through Synthego (Redwood City, CA). The chemical modifications on each sgRNA were 2′-O-methyl analogs and 3′ phosphonothioate internucleotide linkages at the first three 5′ and 3′ terminal RNA residues. The repair template was chemically synthesized by

IDT (Coralville, IA) as a 200bp single-stranded DNA oligo (ssODN). The ssODN was complementary to the non-target strand and contained symmetrical homology arms. An additional silent mutation was introduced for genotyping purposes.

sgRNA sequence: 5′-TCCAGGTGCTGGATCCCAC-3′. Repair template sequence (sgRNA sequence disrupted by desired mutation): 5′-CTGCTGCAGCCTCTCCCCCACTGCTGCAGCCCCAGCCCCACTGCTGCAGCCCCAGCCCCACTGCTGCAGCCCTGATCTTCCTGTTTCTAGGACCTGT**A**G**C**ATCCAGCACCTGGAGCGAGCAGGTGGCAACTTGAACCTGCTGACCTCCTTCTACTTCTGCATCGTGACTTTCTCAACTGTGGGCTTCGGTGATGTGAC -3′. A mix containing a final concentration of 3.0μM sgRNA, 2.0μM enhanced specificity Cas9 protein (Sigma) and 1.6μM ssODN was made immediately prior to electroporation. CRISPR sgRNA/Cas9 RNP complexes were formed by gently mixing the sgRNA and Cas9 protein together and incubating at room temperature for 10 min. After RNP formation, the ssODN repair template was added to the mixture. Using a NepaGene21 electroporator along with a 1.5-mm gap glass slide electrode, zygotes were electroporated under the following conditions: Poring pulse: 40V, 3.5ms length, 50ms interval, 10% decay rate, positive polarity (x4 pulses) Transfer pulse: 5V, 50ms length, 50ms interval, 40% decay rate, alternating polarity (x5 pulses). Manipulated zygotes were then surgically transferred to pseudo-pregnant surrogate CD1 females (8 weeks of age) purchased from Charles River Laboratories (Wilmington, MA). Multiple animals carrying the desired single base pair change were identified by genotype analysis and confirmed by nucleotide sequence analysis of the region around the base pair change. The founders confirmed to carry the mutation were backcrossed to C57BL6/J for 2 generations and then to C57BL6/NJ (Jackson laboratory #005304) for 2 generations to establish the strain C57BL/6NJ *Kcnt1*^{em1Bryd} which is available at the Mutant Mouse

Resource and Research Center at the university of Missouri (MMRRC#075727) and is available upon request at www.nmrrc.org. In spring 2021, animals were transferred to UC Davis, School of Medicine (Sacramento, CA) to establish a colony. This colony was maintained by backcrossing to C57BL/6J for >10 generations.

Genotyping: Genomic DNA was extracted by placing a small amount of tissue (ear or tail) in 100µl alkaline lysis reagent (25mM NaOH and 0. mM EDTA at a pH of 12) and heating at 95 ˚C for 1hr. This was followed by addition of 100µl neutralization buffer (40mM Tris-HCl) with vortexing for 5 seconds to mix. The PCR primers were Kcnt1.F1: 5'-cattccacactgcagccctgtctct-3'and Kcnt1.R1: 5'-caagggtgacacagatcaggatgaccac- 3'. The 25µl reaction contained the following: 12.5µl EmeraldAmp® Supermix (Takara Bio USA Inc., San Jose, CA); 10.0µl H_2O; 0.75µl Forward primer (10µM); 0.75µl Reverse primer (10µM); 1µl genomic DNA (~5-50ng). Thermal cycler conditions were 1) 95 °C, 3 minutes, 2) 95 °C, 30 seconds, 3) 69 °C, 30 seconds, 4) 72 °C, 1 minute. Steps 2-4 were repeated 40 times, 5) 72°C, 7 minutes, 6) 4 °C, hold. The expected PCR amplicon = 403 bp**.** Following PCR amplification, 2.8µl CutSmart buffer and 1.0µl *BtsC*I (20 units) (New England Biolabs, Ipswich, MA) were added directly to the PCR reaction and incubated at 50°C for 2hrs. Gel electrophoresis was performed with a 3% agarose gel in 1X TAE buffer at 80V for 1hr. Expected restriction fragment sizes: wild type allele = 19bp, 23bp, 42bp, and 319bp; mutant allele = 19bp, 23bp, 42bp, 113bp, 206bp. The 319bp fragment in the wild type allele is cut into 113bp and 206bp fragments in the mutant allele.

Cell Culture: Test mice were generated by crossing male and female $Kcnt1^{+/G269S}$ to yield pups of three genotypes ($Kcnt1^{+/+}$, $Kcnt1^{+/G269S}$, and $Kcnt1^{G269S/G269S}$) and neonatal cortices (PND 0-2) were collected. Primary cortical neuron-glia cultures were prepared as previously described (Brewer, 1997; McManus and Brewer, 1997; Hanes et al., 2020; Seiler et al., 2024). Briefly, cortices were

minced with a razor blade prior to incubation in Hibernate A containing papain and DNase. The tissue was then triturated with glass pipettes to dissociate cells from the extracellular matrix (Bellco Glass, Vineland, NJ). Dissociated cells were counted and plated as described below.

High Density Microelectrode Array Plating: MaxWell Biosystems high density microelectrode arrays (HD-MEAs) were used to assess electrophysiological activity of primary neuronal cultures, as previously described (Ben-Shalom et al., 2012; Fenton et al., 2024). MaxTwo 6-well HD-MEA plates were sterilized, filled with 2mL of plating medium (Neurobasal Plus medium (Gibco, ThermoFisher Scientific), 2% B27 Plus supplement (×50) (Gibco, ThermoFisher Scientific), 1x GlutaMAX supplement (Invitrogen), 10% heat-inactivated horse serum (Invitrogen), and HEPES buffer (1M, pH 7.5) (Fisher Scientific)), then incubated for 2 days at 37°C with 5% CO_2. On the day of cell plating, the plating media was removed, and chips washed with sterile water, coated with primary coating (50µl of 0.07% polyethyleneimine (PEI, Sigma-Aldrich)), and incubated for 1hr. The primary coating was removed, the chips were washed 3 times with sterile water, and vacuum dried. Secondary coating (50ul Laminin (0.02 mg/mL; Sigma-Aldrich)) was applied and incubated (~ 1hr) until ready to plate cells. The laminin coating was removed, 50uL of primary cortical cells were added to the HD-MEAs, yielding approximately 125,000 cells per chip, and incubated for 1hr before the addition of 2mL plating medium. 24 hours later, 50% of media was removed and replaced with cell culture maintenance media (Dulbecco's Modified Eagle Medium (DMEM) supplemented with GlutaMax, D-glucose and sodium pyruvate (Gibco, ThermoFisher Scientific) and 10% horse serum). Media changes occurred twice weekly by removing 50% of the media and replacing it with an equal volume of cell culture media. Neural activity was recorded twice a week as described below.

HD-MEA Electrophysiological Recordings and Data Processing: HD-MEA recordings were performed between days *in vitro* (DIV) 3 to 30 to capture the developmental trajectories of dissociated neuronal cultures. Due to differences in recording schedules across experiments, some DIVs varied slightly between litters (e.g., DIV 13 vs 14, DIV 27 vs. 28). Each session began with the Activity Scan Assay, which recorded 30-second segments across the entire chip under 'Sparse 7x' configuration to assess overall activity of the chip. Based on spike amplitude and spatial distribution, 1,020 electrodes were selected from regions exhibiting high activity (spike amplitude) to maximize neuron coverage in the Network Scan Assay. Spontaneous activity was recorded for 300s at a 10 kHz sampling rate using the MaxTwo device (MaxWell Biosystems).

Data processing focused on two aspects: (1) The activity of the culture over time, and (2) network-level dynamics reflecting population synchrony and communication. Raw extracellular signals were bandpass filtered between 300Hz and 3,000Hz to isolate multi-unit activity (MUA). Spike detection was performed using a threshold set at five times the standard deviation of baseline noise. A recording channel was considered active if it exceeded a predefined minimum firing rate and spike amplitude threshold. The mean firing rate and mean spike amplitude were computed from all active channels to assess the overall culture health and neuronal proliferation. To characterize network-level activity, detected spikes were transformed into spike raster plots and binned to generate population firing rates. A Gaussian kernel was applied to these binned spike trains to estimate a continuous measure of population activity, capturing burst dynamics and synchronous events. Statistical comparisons between genotypes were conducted using repeated measures ANOVA over time and one-way ANOVAs followed by tukey's post hoc tests for selected group comparisons. To ensure analytical consistency, adjacent DIVs with ±1 day variation

were grouped during analysis. All analyses were conducted using custom MATLAB R2024 scripts in combination with the MaxWell Biosystems Toolbox (v23.2).

Subjects for developmental milestones, behavioral assays, and seizure susceptibility: All mice were housed in a temperature- and humidity-controlled vivarium maintained on a 12:12 light-dark cycle and tested during the light cycle. Animals were fed a standard diet of Teklad global 18% protein rodent diets 2918 (Envigo, Hayward, CA, USA). Wild-type (WT) and heterozygous *Kcnt1*$^{+/G269S}$ offspring were labeled by paw tattoo over postnatal days (PND) 2-4 using non-toxic animal tattoo ink (Ketchum Manufacturing Inc., Brockville, ON, Canada). Tail biopsies (1–2 mm) from pups were taken for genotyping, following the UC Davis IACUC policy regarding tissue collection. Mice were weaned at PND21, and group housed by sex with 2-4 animals per cage. Assays were performed in order of least to most stressful and between the hours of 9:00 AM PST and 4:00 PM PST during the light phase. All behavior testing was conducted by an experimenter blinded to genotype and included both sexes. Mice were allowed to habituate in their home cages in a dimly lit room adjacent to the testing room for 1hr prior to the start of testing to limit any effect of transporting between the vivarium and testing suite. Between subjects, testing apparatus surfaces were cleaned using 70% ethanol and allowed to dry.

Behavioral Assays: Three cohorts of mice were used for a combination of developmental milestones, seizure-related outcomes, behavioral phenotypes, and respiratory physiology, with full details below. Cohort 1 was used to assess developmental milestones (**Supplemental Table 1**) at PND 3, 5, 9, and 11, behavioral testing order was open field, rotarod, spontaneous alternation in the Y-maze, novel object recognition, contextual and cued fear conditioning and a seizure susceptibility assessment using low stimulus electroconvulsive threshold detection (ECT, Ugo Basile, Gemonio (VA), Italy) and high dose (lethal) chemoconvulsant for seizure susceptibility

with pentylenetetrazol (PTZ, 70mg/kg) intraperitoneally (i.p.). These were not counterbalanced for order of administration because the PTZ dose is lethal, therefore it had to be the "second hit." Cohort 2 comprised 4 litters tested during a critical time window (PND 21-23) for hyperthermia-induced seizures. Finally, Cohort 3 mice comprised of littermates from 8 litters underwent whole body plethysmography (WBP) separated by sex. Body weight/size dictates the volume of air that can be inhaled in the WBP chamber, males are larger than age matched females, thus sexes were separated in the WBP presentation and analysis.

(i) Open field locomotion

Exploratory locomotion in a novel open field environment was assayed in a room illuminated at ~40lux in a 40 cm×40 cm×30.5 cm arena as previously described (Silverman et al., 2013; Copping et al., 2017; Dhamne et al., 2017; Gompers et al., 2017; Adhikari et al., 2022). Exploratory locomotion is an essential assay for gross motor abilities and physical activity over time, identifying key motoric phenotypes, that utilize a conserved neural circuit from flies to humans.

(ii) Rotarod

Motor coordination, balance, and motor learning was assessed using an Ugo-Basile accelerating rotarod (Stoelting Co, Wood Dale, IL) as previously published (Berg et al., 2021; Petkova et al., 2022; Huie et al., 2025). Mice are placed on a rotating cylinder that slowly increases from 4 to 40 revolutions per minute (rpm) over a 5 min trial, with 3 trials per day using a 60min inter-trial interval, repeated over 3 consecutive days for a total of 9 trials. Performance was scored as latency to fall (sec) from the cylinder with a maximum latency of 300sec.

(iii) Whole Body Plethysmography (WBP)

Whole-body plethysmography (WBP) chambers (Buxco, Data Sciences International, St. Paul, MN) were utilized to assess respiratory parameters, such as inhalation/exhalation volumes, as well

as the occurrence and time spent in apneas (an absence of inhaling or exhaling). WBP has been used to show hyperresponsiveness of the airway during allergic reactions (Duarte et al., 2012; Fusco et al., 2021; Alvente et al., 2023).

(iv) Electroconvulsive Seizure Threshold (ECT)

Low intensity (5mA with a 0.9 ms pulse width, 299 Hz, for 200 msec), electroconvulsive shock was administered via ear clamps to assess seizure threshold via a ECT Racine Scale consisting of 0-walks away; 1-brief stun and walks away; 2-very brief jaw, forelimb clonus, lasting less than 1 sec; 3-prolonged jaw, forelimb clonus, ventral or dorsal neck flexion, loss of posture, lasting several seconds; 4-tonic extension of forelimbs (90 degree angle to torso); 5 tonic extension of hind limbs (90 degree angle to torso). The ECT Racine Scale is unique in that animals typically experience a single seizure event resulting in a single score and then recover over time.

(v) Seizure susceptibility by a lethal dose of the chemoconvulsant pentylenetetrazol (PTZ)

Dosing was conducted between 9am-2pm in a well-lit room and followed our validated dosing regimens for C57BL/6J. Subjects were weighed and administered PTZ (70 mg/kg, i.p.), then placed in a clean, empty cage and subsequent seizure stages were live scored using a modified Racine scale for a maximum of 30min. Stages scored were (1) first jerk/Straub's tail, (2) loss of righting reflex (3) generalized clonic-tonic seizure, (4) full tonic extension, (5) death. The PTZ Racine Scale is unique in that animals typically progress through the stages over time beginning with 1 and ending at 5.

(vi) Hyperthermia-induced seizure susceptibility

Subjects were habituated in an adjacent room for at least 30min in low light (~30lux). Subjects were given a brief anesthetic exposure (0.1ml 4% isoflurane for 30s-1min till loss of consciousness), for insertion of rectal temperature probe (Physitemp RET-4, Clifton, NJ, USA),

then placed in the testing arena. A heat lamp is turned on and placed above the arena at a distance to maintain an internal body temperature of 37.5°C for a 10min habituation period. Next, the lamp is moved closer to raise the body temperature by approximately 0.5 degrees every 2min. Testing continues until a behavioral seizure score of 3 or above, or until the body temperature reaches 42.5°C. An observer blind to genotype records the type of seizure using a modified Racine Scale (1. Staring, 2. Head nodding, 3. Unilateral forelimb clonus, 4. Bilateral forelimb clonus, 5. Rearing and falling, 6. Clonic seizure). The febrile Racine Scale is unique in that animals typically progress through the stages over time and then recover once they are removed from the heat source. Animals are returned to their home cage once they are active and mobile and are provided hydrogel (~30min).

Statistical Analysis

Data were analyzed with GraphPad Prism by two tailed Student's t-test for single parameter comparison between the two genotypes, or a One-Way Repeated Measures ANOVA for comparison of genotype over time (*e.g.* development, open field, pre-and post-fear conditioning). Significance levels were set at $p<0.05$. Significant ANOVAs were followed by Bonferroni-Dunn posthoc testing.

Results.

Mouse Model Generation. The *KCNT1* gene sequences differ slightly between human and mouse: the altered amino acid in the G288S human KCNT1 variant is at amino acid position 269 in the mouse protein (**Fig. 1**). Genome editing with CRISPR/Cas9 was used to make the mouse model: the WT mouse *Kcnt1* exon 11 codon (GGG) was replaced with AGC to create the missense mutation. This leads to glycine (G) being replaced by serine (S) at amino acid position 269 (G269S) in the mouse Kcnt1 protein this new allele ($Kcnt1^{em1Bryd}$) was nucleotide sequence verified. The mutation was generated on a C57BL/6J genetic background and was maintained by backcrossing heterozygous animals to B6/J and B6/NJ mice.

High-Density Microelectrode Array Analysis Reveals Distinct Network Activity Patterns in $Kcnt1^{+/G269S}$ and $Kcnt1^{G269S/G269S}$. To investigate the functional consequences of the *Kcnt1* G269S mutation at the network level, we employed high-density microelectrode array (HD-MEA) recordings of primary cortical neurons from wild-type ($Kcnt1^{+/+}$), heterozygous ($Kcnt1^{+/G269S}$), and homozygous ($Kcnt1^{G269S/G269S}$) mice. The Maxwell Biosystems HD-MEA platform featuring 26,400 electrodes with 1,024 simultaneous recording channels enabled detailed spatial and temporal mapping of neuronal network activity patterns (**Fig. 2A**). Extracellular signals were recorded from multiple channels allowing for precise detection of action potentials across the neuronal population (**Fig. 2B, C**) from DIV 13-21, spanning the critical network formation and early maturation phases. To ensure comparable recording conditions across genotypes, we quantified the percentage of active electrodes: all three genotypes showed similar electrode activation rates (approximately 70-75%, **Fig. 2D**), indicating that the G269S mutation did not significantly affect neuronal viability or density during initial plating and attachment. However, despite similar electrode coverage, mean firing rates (DIV13-21) differed significantly between

genotypes (**Fig. 2E;** $F_{(2,168)}$=13.21, p<0.0001) in a gene-dosage dependent manner: *Kcnt1*$^{G269S/G269S}$ neurons had the highest mean firing rate (4.50±0.28 Hz), followed by *Kcnt1*$^{+/G269S}$ (3.56 ± 0.14Hz) and *Kcnt1*$^{+/+}$ neurons (2.84±0.15 Hz). Tukey's post hoc tests revealed that *Kcnt1*$^{G269S/G269S}$ neurons fired significantly more than *Kcnt1*$^{+/G269S}$ (p=0.001) and *Kcnt1*$^{+/+}$ neurons (p<0.0001); while Kcnt1$^{+/G269S}$ neuronal firing rate did not reach significance from *Kcnt1*$^{+/+}$ (p=0.051).

Network Development and Bursting Dynamics. Early network development corresponds to DIV 13 when synchronous activity begins to emerge and spread across the neuronal population (Bikbaev et al., 2015; Cabrera-Garcia et al., 2021), while DIV 27 represents the mature network phase characterized by established bursting patterns and stabilized connectivity (Downes et al., 2012; Spencer et al., 2012; Vertes et al., 2014). At DIV 13, we observed distinctive firing patterns across the three genotypes (**Fig. 3A-C** $F_{(2,52)}$=6.515, p=0.003). During this network formation phase, *Kcnt1*$^{G269S/G269S}$ cultures displayed more frequent bursting activity compared to *Kcnt1*$^{+/+}$ (tukey's post hoc p=0.002), with *Kcnt1*$^{+/G269S}$ networks showing intermediate burst frequency ($tukey_{WTvsHT}$ p=0.039; $tukey_{HTvsHOM}$ p=0.199). By DIV 27, the differences in activity patterns became more pronounced but showed a different trajectory than at DIV 13 (**Fig. 3D-F** $F_{(2,40)}$=14.60, p<0.0001). While *Kcnt1*$^{+/+}$ and *Kcnt1*$^{+/G269S}$ cultures maintained consistent bursting patterns with increased synchronization characteristic of mature networks, *Kcnt1*$^{G269S/G269S}$ cultures exhibited markedly diminished burst amplitude and altered burst patterns ($tukey_{WTvsHOM}$ p=0.149; $tukey_{HTvsHOM}$ p<0.0001). This unexpected reversal in the homozygous phenotype suggests potential network dysfunction emerging with prolonged exposure to hyperexcitability, possibly through excitotoxic mechanisms.

Temporal Evolution of Network Hyperexcitability. Quantitative analysis of burst frequency across developmental timepoints (**Fig. 3G** $F_{TIME(2,109)}$=7.516, p=0.0003; $F_{GENOTYPE(2,52)}$=8.027,

p=0.0009) revealed a striking biphasic pattern in *Kcnt1*$^{G269S/G269S}$ cultures. Between DIV 13-17, *Kcnt1*$^{G269S/G269S}$ networks exhibited significantly higher burst counts (107.9± 7.21) per recording, compared to *Kcnt1*$^{+/+}$ (62.00 ± 7.41, tukey's p=0.002) reflecting initial hyperexcitability during network formation. However, bursting activity declined in *Kcnt1*$^{G269S/G269S}$ networks (87.19± 7.31) with frequency falling below *Kcnt1*$^{+/+}$ levels (108.4± 5.34) by DIV 24-27 ($F_{(2,40)}$=9.77, p=0.0004; tukey's p=0.162). In contrast, *Kcnt1*$^{+/G269S}$ cultures increased burst frequency over development, showing significantly elevated activity (95.15±4.74; tukey's p=0.0003) at DIV13-17 compared to *Kcnt1*$^{+/+}$ and rising to *Kcnt1*$^{+/+}$ levels (129.40±6.91 tukey's p=0.121) by DIV 24-27. Meanwhile, *Kcnt1*$^{+/G269S}$ cultures burst frequency was below *Kcnt1*$^{G269S/G269S}$ networks at DIV 13-17 (tukey's p=0.275) and rose above their levels by DIV 24-27 (tukey's p=0.0002). This indicates that the *Kcnt1*$^{+/G269S}$ confers a persistent and sustainable hyperexcitability phenotype that remains compatible with ongoing network function, unlike *Kcnt1*$^{G269S/G269S}$.

Further analysis of the firing pattern variability using the Fano factor, the variance-to-mean ratio of spike counts, a higher Fano factor reflects the healthy stochastic variability essential for proper circuit formation and refinement (Wagenaar et al., 2006; Mochizuki et al., 2016). *Kcnt1*$^{+/+}$ networks maintained high Fano factor values (**Fig. 3H,** 656.31 ± 71.94; DIV 13 $F_{(2,51)}$=7.057, p=0.002; DIV 27 $F_{(2,39)}$=12.36, p<0.0001). In contrast, both *Kcnt1*$^{G269S/G269S}$ (303.11 ± 32.09; tukey's p=0.004;) and *Kcnt1*$^{+/G269S}$ networks (326.67 ± 28.08; tukey's p=0.003) showed significantly lower values during early network formation DIV 13. While the Fano factor of *Kcnt1*$^{+/G269S}$ networks gradually increased toward *Kcnt1*$^{+/+}$ levels by DIV 27 (tukey's p=0.253), *Kcnt1*$^{G269S/G269S}$ networks remained locked in an abnormally regularized firing pattern (tukey's p<0.001). This developmental trajectory—initial hyperexcitability followed by progressive reduction in network activity in *Kcnt1*$^{G269S/G269S}$ cultures, contrasted with sustained

hyperexcitability in *Kcnt1*$^{+/G269S}$ cultures—suggests that the G269S GOF mutation affects network development in a gene-dosage dependent manner. Based on these electrophysiological findings, we decided to pursue only the *Kcnt1*$^{+/G269S}$ model for subsequent *in vivo* behavioral characterization.

Exploratory locomotion and motor coordination in the G288S Kcnt1*$^{+/G269S}$ *mouse model.

Novel exploration in the open field was assessed between age, sex matched littermates, for effects resulting from *Kcnt1*$^{+/G269S}$. Total activity across a 30-minute session illustrated an effect over time in both genotypes (**Fig. 4A**; $F_{time\ (3,\ 148)}=7.706$, $p<0.0001$), showing acclimation to the arena, as expected. A trend toward hyperactivity in the *Kcnt1*$^{+/G269S}$ was observed (**Fig. 4A**; $F_{(1,\ 42)}=0.6074$, $p=0.4404$) when the 30-minute session was summed (**Fig. 4B**; $t_{(1,\ 40)}=2.156$, $p=0.0372$). Motor coordination and motor learning were measured using the accelerating rotarod. We observed a significant reduction in latencies to fall in *Kcnt1*$^{+/G269S}$ compared to *Kcnt1*$^{+/+}$ age matched mice (**Fig. 4C**; $F_{genotype(1,\ 42)}=6.79$, $p=0.0126$) indicating poor motor coordination. However, over the three training days we observed improved performance over time, (**Fig. 4C**; $F_{time(2,\ 84)}=36.05$, $p<0.0001$), in both genotypes illustrating intact motor learning.

Cognitive ability assessed by two standardized assays in the Kcnt1*$^{+/G288S}$ *mouse model is intact.

Cognitive ability was assessed in 2 different tasks novel object recognition (NOR) memory and fear conditioning. During the familiarization phase of the NOR task, Kcnt*1*$^{+/G269S}$ animals explored the objects substantially less than the *Kcnt1*$^{+/+}$ control mice (**Fig. S1A**: $F_{familiarization\ genotype\ (1,\ 29)} = 0.00306$, $p < 0.0001$), with a mean investigation time in *Kcnt1*$^{+/+}$ subjects of 52.285 sec, while in *Kcnt1*$^{+/G269S}$ the mean investigation time was 26.865 sec. During the novel investigation phase, both genotypes spent greater time investigating the novel object, versus the familiar object (**Fig. S1B** =: $F_{WT\ (1,\ 41)}=4.813$, $p<0.05$ and $F_{Kcnt1+/G269S\ (1,\ 36)}=18.50$, $p<0.001$). The discrimination index

was calculated by dividing the difference in investigation time between the novel and familiar object by the total amount of exploration of both objects (**Fig. S1C**: $t_{(1, 40)}$=0.7566), clearly illustrating a lack of cognitive impairments in this assay. Cued and contextual fear conditioning illustrated a strong effect of training (learning from the tone-shock pairings (UCS-CS) (**Fig. S1D**; $F_{training\ (1, 40)}$=107.8, p<0.0001). While a genotype by training interaction was observed, (**Fig. S1D**; $F_{training\ x\ genotype\ (1, 40)}$=4.951, p<0.04), no genotype effect, during training, was observed, (**Fig. S1D**; $F_{genotype\ (1, 40)}$=0.7672, p=0.3863), which is a key control, no effect on training allows us to investigate for differences in memory and recall. Contextual recall 24 hrs. after UCS-CS training did not differ between genotypes (**Fig. S1E**; $t_{(1, 50)}$= 0.4610, p=0.6468). However, uniquely, cued recall, performed 48hrs after initial training, illustrated recall of the cued-shock pairing by high levels of freezing illustrated post cue but not pre cue. Moreover, cued recall, exhibited pronounced elevated freezing post cue, in *Kcnt1*$^{+/G269S}$ compared to WT age matched mice (**Fig. S1F**; $F_{cue\ (1, 40)}$=11.05, p<0.0001).

Behavioral seizure quantification, as induced by 3 different methodologies at 2 different ages in the G288S Kcnt1$^{+/G269S}$ mouse model. Seizures were measured in 2 ways in cohort 1 animals after completion of behavioral assays and a 3rd method was used in cohort 2. Firstly, in cohort 2 susceptibility to seizures early in life (post-natal day 21-23), induced by hyperthermia, analogous to fever induced (febrile) seizures, was measured for probability to develop behavioral seizures, temperature to first seizure, and severity of seizure as measured by a modified Febrile Racine score. *Kcnt1*$^{+/G269S}$ animals had a higher average Febrile Racine score than *Kcnt1*$^{+/+}$ controls (**Fig. 5A**: $t_{(1, 31)}$ = 2.146, p < 0.05) and a lower temperature threshold (**Fig. 5B**: t (1, 16) = 2.849, df=16, p < 0.01). *Kcnt1*$^{+/G269S}$ animals also had an increased probability of developing a behavioral seizure (**Fig. 5C**: $\chi 2$ = 7.506, p < 0.0005), over their *Kcnt1*$^{+/+}$ counterparts. Seizures in cohort 1 animals

were first induced by ear-clip electroconvulsive threshold (ECT) wherein animals reached similar seizure levels (**Fig. 5D**: $t_{(1, 40)}$ =0.17, p = 0.86) and recovered post-seizure induction in less than 5 minutes (**Fig. 5E**: $t_{(1, 37)}$=1.28, p=2.08). Both *Kcnt1*$^{+/G269S}$ and *Kcnt1*$^{+/+}$ animals had similar probability of recovery post-seizure experience (**Fig. 5F**: $\chi 2$ = 7.506, p=0.65). Following PTZ administration at 70 mg/kg, a lethal dose, *Kcnt1*$^{+/G269S}$ and *Kcnt1*$^{+/+}$ mice reached each seizure stage at similar rates (**Fig. 5G**: $F_{(1,37)}$=0.01, p=0.92), including latency to first jerk, latency to loss of righting, latency to generalized clonic-tonic seizure, latency to full extension, and latency to death. Additionally, the probability of survival was similar between *Kcnt1*$^{+/G269S}$ and *Kcnt1*$^{+/+}$ animals (**Fig. 3H**: $F_{(1,12)}$=0.499, p=0.49). Taken together, the *Kcnt1*$^{+/G269S}$ animals were highly sensitive to early life heat-induced seizures, as opposed to the adult exposure to either electroconvulsive or chemoconvulsive induced seizures. Since the ECT and PTZ seizure inductions were conducted in the same animals we correlated the seizure severity between the two induction methods, in order to determine if one would be predictive of the other, i.e., correlation (**Fig. S3**). Latency to first jerk after PTZ administration was negatively correlated with seizure severity in ECT in *Kcnt1*$^{+/+}$ animals (**Fig. S3A** r=-0.46, p=0.05). While latency to generalized tonic-clonic PTZ seizures were negatively correlated with seizure severity after ECT in *Kcnt1*$^{+/G269S}$ (**Fig S3G** r=-0.57, p=0.02). Together these correlations indicate that mice that experienced the most intense responses to ECT, also moved more quickly through the Racine scale stages during PTZ induced seizures.

Respiratory parameters identified erratic breathing and apnea in the Kcnt1$^{+/G288S}$ mouse model. Our laboratory was interested in defining respiratory metrics at baseline, given KCNT1-related epilepsy's increased incidence of Sudden Unexpected Death in Epilepsy (SUDEP) and elevated apneas (Moller et al., 2015; Kuchenbuch et al., 2019; Chorny et al., 2024). Animals were assessed

for 2hrs during the light cycle for respiratory parameters in the whole-body plethysmography (WBP) chambers. *Kcnt1*$^{+/G269S}$ and *Kcnt1*$^{+/+}$ breathing characteristics including inspiration and expiration volumes, as well as the presence of apneas were quantified. Animals were separated by sex as aged matched female mice are smaller than their male counterparts resulting in inherent sex differences for these measures. Percentage of time spent breathing normal was similar between *Kcnt1*$^{+/G269S}$ and *Kcnt1*$^{+/+}$ females (**Fig. 6A**: $t_{(1, 18)}$=0.4896, p=0.6297) while decreased normal breathing was observed in males (**Fig. 6A**: $t_{(1,17)}$=2.391, p=0.0258). Additionally, males and females of both genotypes had similar levels of erratic breathing (**Fig. 6B**: females $t_{(1, 18}$ =1.675, p=0.1094; males $t_{(1,17)}$=0.7847, p=0.4410). Lastly, the number of apnea events was elevated in *Kcnt1*$^{+/G269}$ mice in males (**Fig. 6C**: $t_{(1, 17),}$t=2.391, p=0.0258) and not in females (**Fig. 6C**: $t_{(1, 18),}$t=0.4896, p=0.6297), compared to their respective sex matched *Kcnt1*$^{+/+}$ controls. Taken together, these data indicate that male *Kcnt1*$^{+/G269S}$ mice experience more respiratory difficulties than age matched females.

Discussion.

Herein, we generated a novel experimental model for *KCNT1*-related epilepsy and channelopathies, a subgroup of neurodevelopmental disorders. Our novel mouse strain carries the mouse equivalent of the human GOF variant G288S. First, CRISPR/Cas9 was used in C57BL/6J mice to replace the wild-type gene codon GGG with AGC, creating the missense mutation of glycine (G) to serine (S) at amino acid position 269 in the mouse Kcnt1 protein. The new allele ($Kcnt1^{em1Bryd}$) was nucleotide sequence verified, and the mice were maintained on B C57BL6/NJ 6/NJ and were donated to the Mutant Mouse Resource and Research Center (MMRRC:075727-MU). Given that other mouse models of developmental epileptic encephalopathy (DEE) and/or rare genetic NDDs, have been made on C57BL/6J, we backcrossed onto C57BL6/J, for research rigor, reproducibility and consistency, despite reported issues with this background strain for seizure models (Frankel et al., 2001; Yang and Frankel, 2004; Miller et al., 2014; Mistry et al., 2014; Copping et al., 2019; Sukoff Rizzo et al., 2020). Future experiments may return to the C57BL6/NJ background strain, given these extensive reports and the sub strain's responsivity relating to spontaneous recurring seizures (SRS), seizure induction (Copping et al., 2019; Calsbeek et al., 2021) and our need to understand the contribution of the background to the phenotype, when testing potential therapeutics (Sittig et al., 2016), as it relates to generalization.

Next, in vitro experiments using primary cortical neurons revealed contrasting gene-dose dependent patterns—initial hyperexcitability followed by network collapse in $Kcnt1^{G269/G269S}$ cultures versus sustained hyperexcitability in $Kcnt1^{+/G269S}$ networks. Most striking, was the ~50% reduction in firing pattern variability (Fano factor: WT ~656 vs. mutants ~300-327) in both mutant genotypes compared to wild-type networks, indicating abnormally regularized activity that

disrupts the stochastic variability required for proper circuit development (Wagenaar et al., 2006). This aligns with established cell type-specific effects where *Kcnt1* gain-of-function variants disproportionately impact inhibitory neuron function, particularly non-fast-spiking GABAergic interneurons (Shore et al., 2020; Wu et al., 2024). The G288S/G269S mutation, located in the channel pore region, has severe impact with homozygous cultures reaching unsustainable network perturbation levels that likely trigger excitotoxic mechanisms—excessive neuronal firing leading to progressive cell death, as evidenced by the elimination of bursting activity by DIV 28. Critically, our heterozygous model maintains persistent but viable hyperexcitability, better representing the human condition and providing a novel platform for therapeutic development. These findings suggest that approaches targeting improved inhibitory tone and excitation-inhibition balance, rather than KCNT1 channel blockade alone, may prove more effective for treating *KCNT1*-related epilepsies (Numis et al., 2018; Xu et al., 2022; Liu et al., 2023).

Next, we discovered that *Kcnt1*$^{+/G269S}$ mice exhibited seizures following early life hyperthermia, a preclinical assay utilized as an analog for febrile seizures or seizures resulting from high temperature fevers (Born et al., 2021). *Kcnt1*$^{+/G269S}$ hyperthermia induced seizures were characterized by onset at lower temperatures compared to age matched control littermates. Also, a higher percentage of *Kcnt1*$^{+/G269S}$ subject mice experienced a seizure, and with higher severity scores, using a modified febrile Racine Scale, compared to age matched control littermates. In contrast, adult mice, given electroconvulsive threshold shock (ECT) to induce seizures, followed by a lethal dose of pentylenetetrazol to induce seizures (PTZ 70mg/kg), using a two-hit paradigm were indistinguishable between *Kcnt1*$^{+/G269S}$ and *Kcnt1*$^{+/+}$ controls, on every assessed metric. Finally, we performed a tailored behavioral phenotyping battery on naïve cohorts of *Kcnt1*$^{+/G269S}$ and *Kcnt1*$^{+/+}$ littermates that included developmental milestones of physical growth and

neurological reflexes, exploratory locomotion, motor coordination and motor learning, novel object learning and memory, and contextual and cued learning and memory. We also gathered information on respiratory physiological parameters using whole body plethysmography (WBP), between *Kcnt1*$^{+/G269S}$ and *Kcnt1*$^{+/+}$, given reports of asthma and pulmonary hemorrhage in patients with *KCNT1*-related epilepsy. While *Kcnt1*$^{+/G269S}$ and *Kcnt1*$^{+/+}$ littermates were developmentally indistinguishable, *Kcnt1*$^{+/G269S}$ mice were hyperactive in the 30min open field arena exploration and lacked motor coordination on days 1 and 2 on the rotarod, illustrated by a reduced latency to fall from the accelerating beam. Finally, *Kcnt1*$^{+/G269S}$ mice exhibited increased apneas and erratic breathing which aligns with the clinical presentation.

In summary, our novel mouse model, reported for the first time herein, backcrossed onto the C57BL6/J background strain, represents an important advancement in the field of *KCNT1*-related epilepsy, DEEs and/or NDD channelopathies. Moreover, we have begun to demystify the role of the C57BL6/J in its typical lack of seizure responsivity and high seizure resistance compared to its closely related sub strains, as well as other congenic inbred strains (Yang and Frankel, 2004; Miller et al., 2014; Copping et al., 2019; Sukoff Rizzo et al., 2020).

Furthermore, we hypothesize that mice who experience an early-life seizure as described herein, would lead to better alignment with clinical characteristics including motor hyperactivity, learning and memory difficulties, apneas, adult seizures, and sleep disturbances. Importantly, assessment of homozygous *Kcnt1*$^{G269S/G269S}$ is not required for translational research making this model ideal for translational therapeutic assessment, *in vitro* and *in vivo*. Targeted therapeutics that may restore inhibitory tone, reduce potassium efflux and/or restore E/I imbalance, over specific channel GOF variants and channel inhibition, as that strategy via quinidine has not proved uniformly useful clinically.

A limitation of the current study and key future study will be to collect wireless electroencephalography (EEG), as performed routinely by our laboratory and others focused on EEG as a translational biomarker for the clinical pipeline (Dhamne et al., 2017; Adhikari et al., 2021; Copping and Silverman, 2021; Haigh et al., 2021; Fenton et al., 2024), especially given the nuance of the C57BL6/J background strain (Purtell et al., 2018). These next steps will document cortical activity characteristics including spiking, spike trains, sleep stages, quantity and quality and spectral power density over several days. A second noteworthy observation is that our adult electroconvulsive threshold experiments were performed using ear clamps and at low intensity. With recommendations from the Frankel laboratory (personal communication), we had our ECT apparatus modified for transcorneal stimulation and higher stimulus intensities, which will be utilized in future research, as preliminary data suggest the severity of this GOF variant requires deeper phenotyping, *in vivo*, and will provide a more comprehensive understanding among the disseminated data on human variants, which will yield improvements for patient stratification.

The G288S mutation was identified by whole exome sequencing (WES) in two *de novo* unrelated patients with early DEE first reported by Rizzo et al. (Rizzo et al., 2016). As introduced earlier, G288S/G269S does not result in a single subtype of *KCNT1*-related epilepsy (Andreone et al., 2025), thus understanding how G288S/G269S modulates network excitability *in vitro* and *in vivo*, might yield information relevant to the most affected individuals and inform stratification for therapeutic development. Groundwork in *KCNT1*-related epilepsy was outlined by many, but we must highlight generous contributions and personal communication with the Wayne Frankel laboratory (Columbia University) who generated the first ever mouse models, the knock-in (KI), human variants Y777H and Y796H and illustrated motor cortex hyperexcitability, early-onset seizures, and hyperactivity in KI/KI mice (Shore et al., 2020). In 2024, Wu et al. discovered the

R455H mutation which exhibited increased sodium conductance, increased excitatory neuron activity, and suppression of excitability in inhibitory interneurons in a mouse model, which altered sodium channel expression (Wu et al., 2023), with effect sizes of 4-6-fold increases in KI/KI mice. While previous findings in homozygous variant mice are significant, with substantial effect sizes to test for therapeutic reversal, there remains an unmet need for a more construct valid single copy KI variant model, since affected individuals with *KCNT1*-related epilepsy are heterozygous. The model presented herein has filled this unmet need by its generation and clear phenotypic excitability in cortical neurons and early life heat seizure sensitivity as an *in vivo* outcome measure, malleable for future therapeutic testing.

Conclusions

Overall, characterization of *Kcnt1*$^{+/G269S}$ mice indicates a sensitivity to hyperthermia-induced seizures and a motor learning delay. Future studies are required to investigate the impact of early life seizures on adult motor, cognitive, and sleep measures as well as EEG before developing novel therapeutic interventions for individuals with *KCNT1*-related epilepsy.

Figure 1. Generation of the *Kcnt1*^{G269S} mutant mouse model.

A) The KCNT1 protein consists of six hydrophobic transmembrane segments with a pore loop domain between the last two transmembrane segments. It also has a large intracellular carboxy-terminal region containing tandem RCK domains and an NAD+ binding domain. The mouse G269S (corresponding to human G288S) mutation, indicated by a red star, occurs within the channel pore. **B)** The mouse model was engineered using CRISPR-Cas9 genome editing to replace the endogenous GGG (Gly) with AGC (Ser). **C)** Confirmation of the engineered DNA base pair changes using Sanger sequencing. The heterozygous sample in the chromatogram shows overlapping G (black) and A (green) peaks for the G to A change and overlapping G (black) and C (blue) peaks for the G to C change.

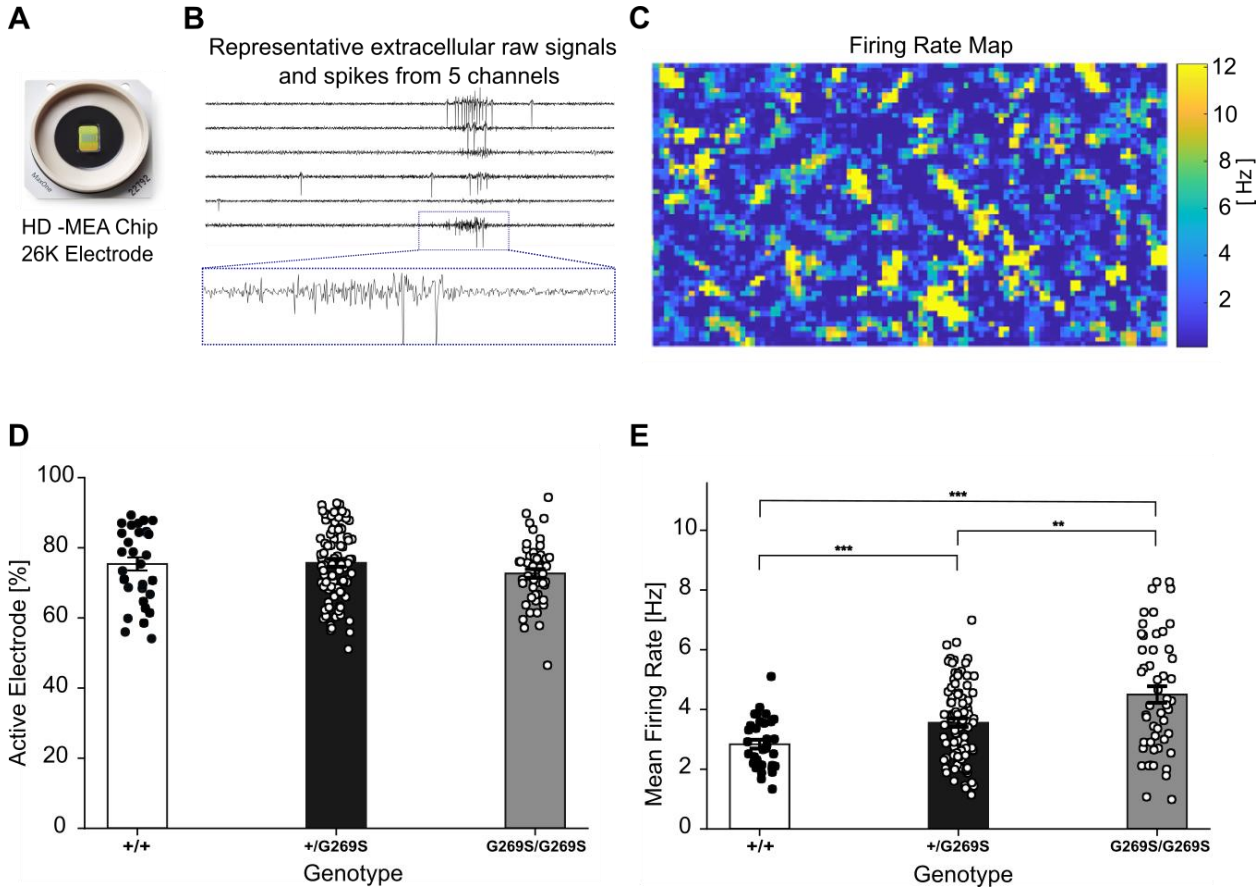

Fig. 2. High-density MEA recordings reveal genotype-dependent differences in neuronal network activity.

(A) Image of the high-density microelectrode array (HD-MEA) chip used in this study (26,000 electrodes; MaxOne platform, Maxwell Biosystems). (B) Example of raw extracellular action potential (eAP) traces recorded from active electrodes. (C) Representative firing rate map from a cortical culture, showing spatial distribution of neuronal activity across the MEA surface. Warmer colors indicate higher firing rates (color scale: 2–12 Hz). (D) Percentage of active electrodes per well for wild-type *Kcnt1*$^{+/+}$, heterozygous *Kcnt1*$^{+/G269S}$, and homozygous *Kcnt1*$^{G269S/G269S,}$ neuronal networks. (E) Quantification of mean firing rate (Hz) across genotypes. *Kcnt1*$^{G269S/G269S}$ neurons fired significantly more than both *Kcnt1*$^{+/G269S}$ ($t = -3.00$, $p = 0.0036$, **) and *Kcnt1*$^{+/+}$($t = 5.27$, $p < 0.0001$, ***), while *Kcnt1*$^{+/G269S}$ neurons also differed significantly from *Kcnt1*$^{+/+}$ ($t = 3.51$, $p = 0.0007$, ***). Bars represent mean ± SEM; individual points reflect biological replicates.

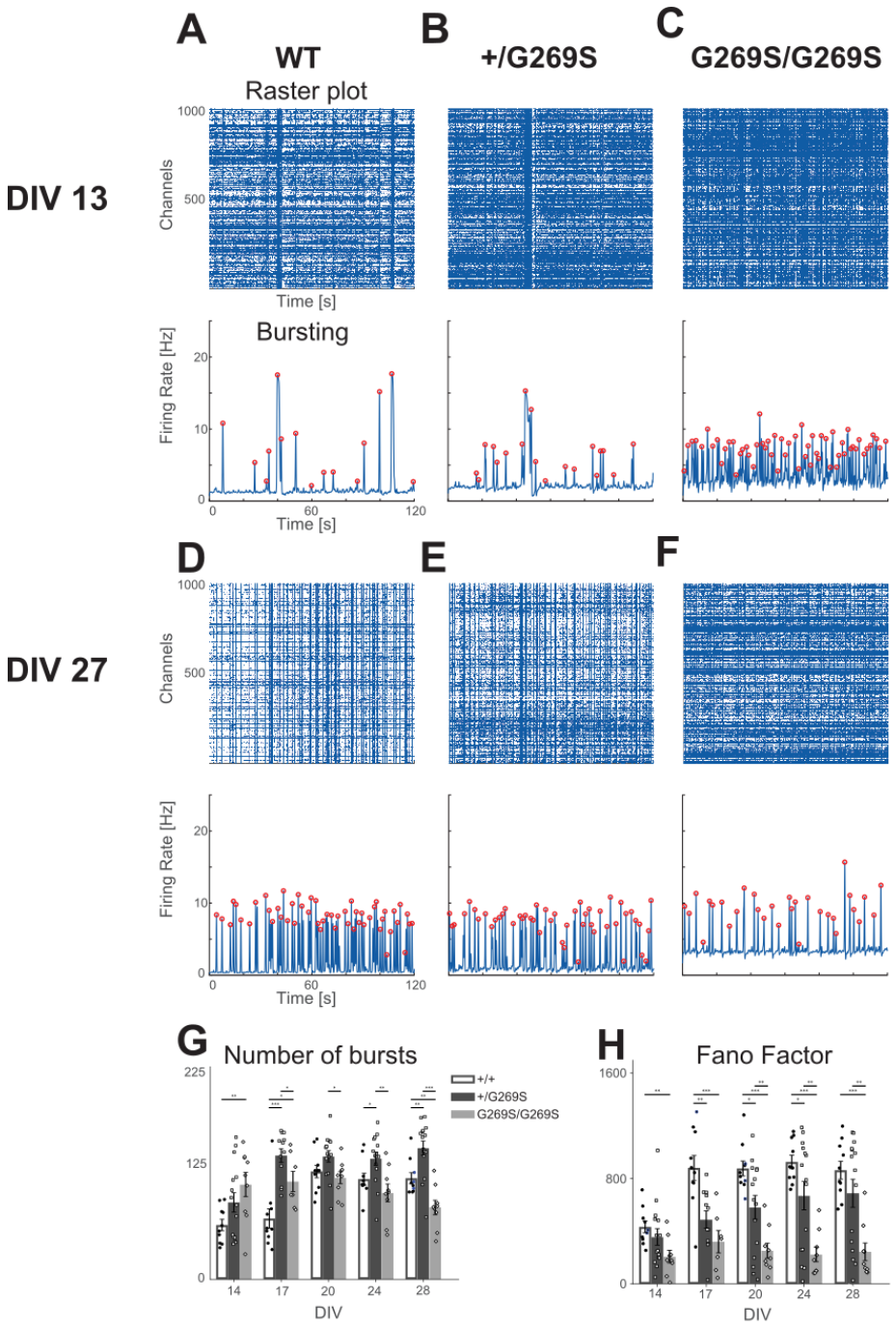

Fig. 3. Developmental progression of burst dynamics in *Kcnt1*$^{+/+}$, *Kcnt1*$^{+/G269S}$, and *Kcnt1*$^{G269S/G269S}$ in primary neuron culture.

(A–F) Representative raster plots (top) and population firing rate traces (bottom) from wild-type (*Kcnt1*$^{+/+}$, A, D), heterozygous (*Kcnt1*$^{+/G269S}$, B, E), and homozygous (*Kcnt1*$^{G269S/G269S}$, C,F) cortical networks recorded at DIV13 (A–C) and DIV27 (D–F). Each raster shows 120 seconds of activity across 1024 electrodes. Firing rate traces display synchronized burst events detected using a Gaussian kernel convolution; red dots indicate burst peaks. *Kcnt1*$^{+/+}$ and *Kcnt1*$^{+/G269S}$ networks display sparse, periodic bursts at DIV13 that become more frequent and structured by DIV27. In

contrast, *Kcnt1*$^{G269S/G269S}$ networks show highly frequent and irregular bursting at DIV13, followed by diminished activity and synchrony at DIV27. (G) Quantification of burst count across developmental timepoints (DIV13–27). *Kcnt1*$^{G269S/G269S}$ networks display a biphasic pattern with early hyperexcitability (DIV13–17) and later hypoactivity, whereas *Kcnt1*$^{+/G269S}$ cultures maintain and increase burst frequency over the developmental time. (H) Fano factor, a measure of firing variability, is significantly reduced in both mutant genotypes compared to *Kcnt1*$^{+/+}$ at all timepoints, indicating abnormally regularized activity. Bars represent mean ± SEM; individual data points represent biological replicates. Error bars indicate mean +/- SEM. $p < 0.05$ (*), $p < 0.01$ (**), $p < 0.001$ (***).

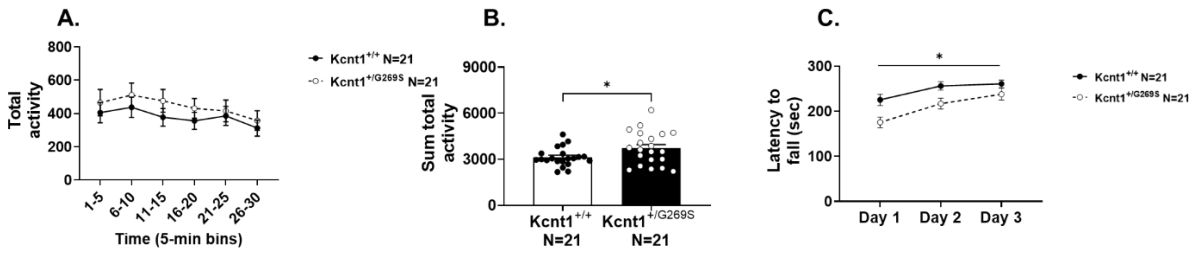

Fig. 4. Elevated motor activity in a novel open field arena using the total activity parameter over a 30-min period in *Kcnt1*$^{+/G269S}$ vs ***Kcnt1*$^{+/+}$.** Gross motor abilities were assessed using activity in a novel open field arena by: A, B) total activity across a 30-min session. In Panel A, data are shown in 5-min bins. C) *Kcnt1*$^{+/G269S}$ have poor motor coordination compared to WT controls using the standard accelerating rotarod paradigm. Error bars indicate mean +/- SEM. * $p<0.05$

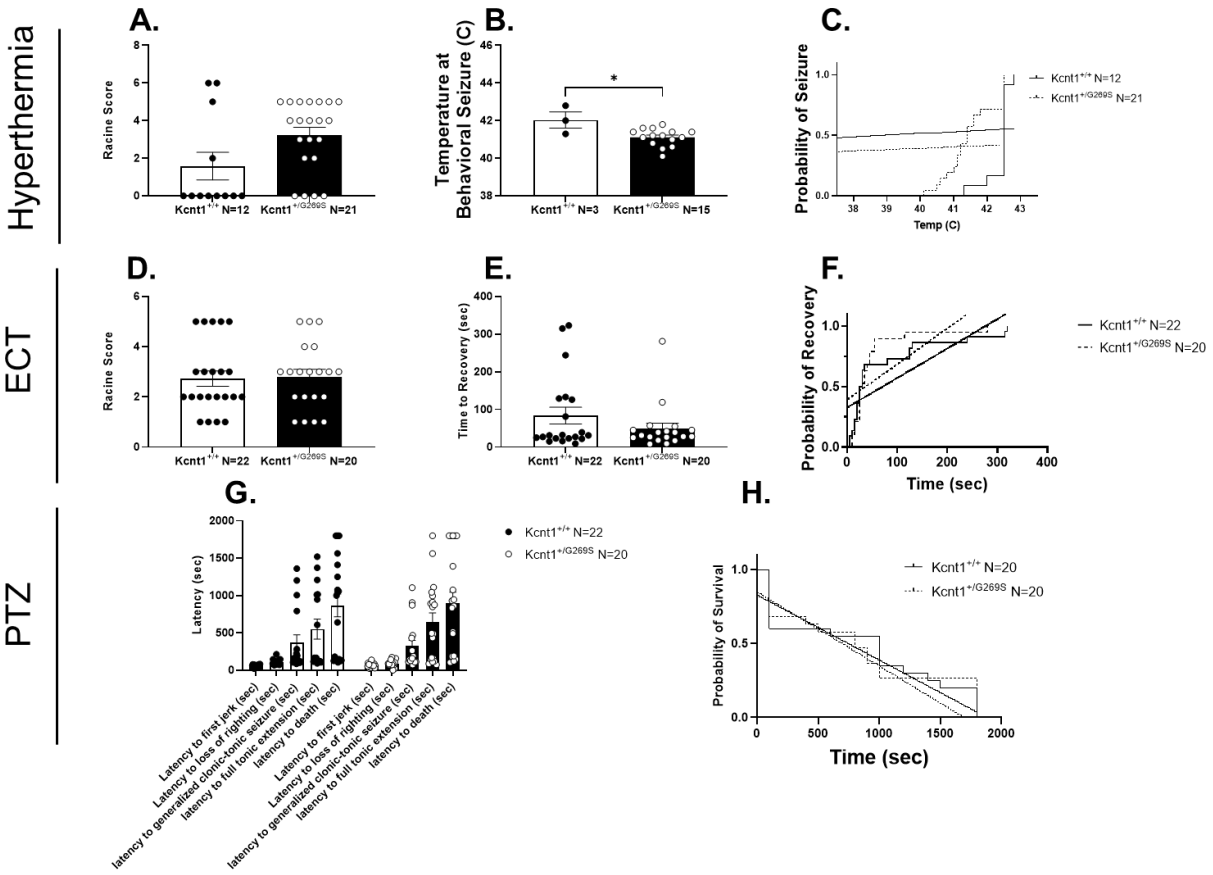

Figure 5: Seizure responsiveness to Hyperthermia-, Electroconvulsive-, and Chemoconvulsive-induction.

A) Seizure severity using modified Febrile Racine scale to Hyperthermia-induced seizure. B) Average temperature to behavioral seizure. C) Probability of behavioral seizure as temperature is increased. D) Seizure severity using a modified ECT Racine scale in response to electroconvulsive shock threshold (ECT; 5mA with a 0.9ms pulse width, 299 Hz, for 200 msec). E) Time to recovery (sec) post ECT induction. F) Probability of recovery post ECT. G) Latency to each stage of a modified Racine scale in response to chemoconvulsive treatment with pentylenetetrazole (PTZ, i.p., 70 mg/kg). H) Probability of survival post PTZ. Error bars indicate mean +/- SEM. * $p<0.05$.

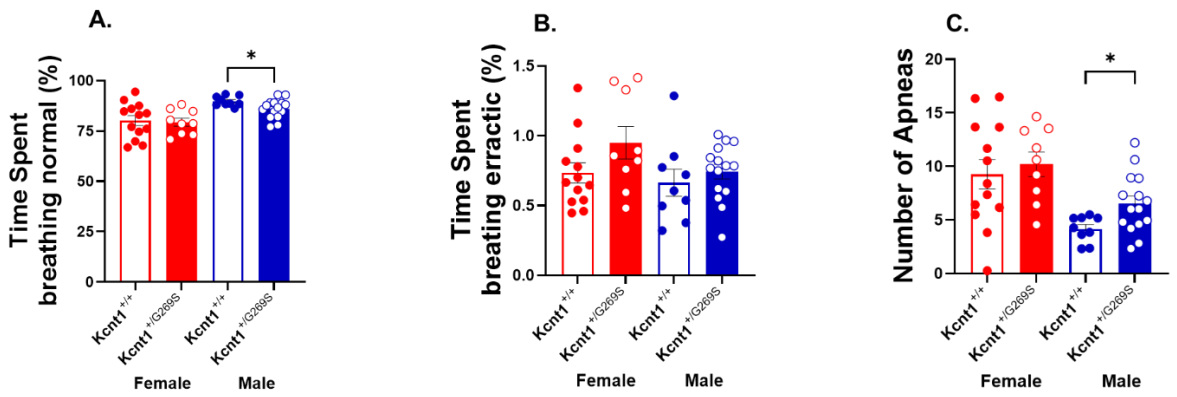

654
655 **Fig. 6: Respiratory apneas and erratic breathing assessed by whole body plethysmography**
656 **(WBP) in *Kcnt1*$^{+/G269S}$ and *Kcnt1* $^{+/+}$ mice.** Whole body plethysmography evaluation for A) % of
657 time breathing normal, B) % of Time breathing erratic, C) number of apneas. Error bars indicate
658 mean +/- SEM. * $p<0.05$
659

References

Adhikari A, Buchanan FKB, Fenton TA, Cameron DL, Halmai J, Copping NA, Fink KD, Silverman JL (2022) Touchscreen cognitive deficits, hyperexcitability and hyperactivity in males and females using two models of Cdkl5 deficiency. Hum Mol Genet 31:3032-3050.

Alvente S, Matteoli G, Miglioranza E, Zoccoli G, Bastianini S (2023) How to study sleep apneas in mouse models of human pathology. J Neurosci Methods 395:109923.

Andreone BJ et al. (2025) Durable suppression of seizures in a preclinical model of KCNT1 genetic epilepsy with divalent small interfering RNA. Epilepsia 66:1677-1690.

Ben-Shalom R, Aviv A, Razon B, Korngreen A (2012) Optimizing ion channel models using a parallel genetic algorithm on graphical processors. J Neurosci Methods 206:183-194.

Berg EL, Petkova SP, Born HA, Adhikari A, Anderson AE, Silverman JL (2021) Insulin-like growth factor-2 does not improve behavioral deficits in mouse and rat models of Angelman Syndrome. Mol Autism 12:59.

Bikbaev A, Frischknecht R, Heine M (2015) Brain extracellular matrix retains connectivity in neuronal networks. Sci Rep 5:14527.

Bonardi CM et al. (2021) KCNT1-related epilepsies and epileptic encephalopathies: phenotypic and mutational spectrum. Brain 144:3635-3650.

Born HA, Martinez LA, Levine AT, Harris SE, Mehra S, Lee WL, Dindot SV, Nash KR, Silverman JL, Segal DJ, Weeber EJ, Anderson AE (2021) Early Developmental EEG and Seizure Phenotypes in a Full Gene Deletion of Ubiquitin Protein Ligase E3A Rat Model of Angelman Syndrome. eNeuro 8.

Brewer GJ (1997) Isolation and culture of adult rat hippocampal neurons. J Neurosci Methods 71:143-155.

Bryda EC (2013) The Mighty Mouse: the impact of rodents on advances in biomedical research. Mo Med 110:207-211.

Burbano LE, Li M, Jancovski N, Jafar-Nejad P, Richards K, Sedo A, Soriano A, Rollo B, Jia L, Gazina EV, Piltz S, Adikusuma F, Thomas PQ, Kopsidas H, Rigo F, Reid CA, Maljevic S, Petrou S (2022) Antisense oligonucleotide therapy for KCNT1 encephalopathy. JCI Insight 7.

Cabrera-Garcia D, Warm D, de la Fuente P, Fernandez-Sanchez MT, Novelli A, Villanueva-Balsera JM (2021) Early prediction of developing spontaneous activity in cultured neuronal networks. Sci Rep 11:20407.

Calsbeek JJ, Gonzalez EA, Boosalis CA, Zolkowska D, Bruun DA, Rowland DJ, Saito NH, Harvey DJ, Chaudhari AJ, Rogawski MA, Garbow JR, Lein PJ (2021) Strain differences in the extent of brain injury in mice after tetramethylenedisulfotetramine-induced status epilepticus. Neurotoxicology 87:43-50.

Chorny LE, Nordli DR, 3rd, Galan F (2024) Breath-holding spells: A typical case with EEG and video correlate. Epileptic Disord.

Copping NA, Adhikari A, Petkova SP, Silverman JL (2019) Genetic backgrounds have unique seizure response profiles and behavioral outcomes following convulsant administration. Epilepsy Behav 101:106547.

Copping NA, Christian SGB, Ritter DJ, Islam MS, Buscher N, Zolkowska D, Pride MC, Berg EL, LaSalle JM, Ellegood J, Lerch JP, Reiter LT, Silverman JL, Dindot SV (2017) Neuronal overexpression of Ube3a isoform 2 causes behavioral impairments and neuroanatomical pathology relevant to 15q11.2-q13.3 duplication syndrome. Hum Mol Genet 26:3995-4010.

Dhamne SC, Silverman JL, Super CE, Lammers SHT, Hameed MQ, Modi ME, Copping NA, Pride MC, Smith DG, Rotenberg A, Crawley JN, Sahin M (2017) Replicable in vivo physiological and behavioral phenotypes of the Shank3B null mutant mouse model of autism. Mol Autism 8:26.

Downes JH, Hammond MW, Xydas D, Spencer MC, Becerra VM, Warwick K, Whalley BJ, Nasuto SJ (2012) Emergence of a small-world functional network in cultured neurons. PLoS Comput Biol 8:e1002522.

Duarte T, Martin C, Baud FJ, Laprevote O, Houze P (2012) Follow up studies on the respiratory pattern and total cholinesterase activities in dichlorvos-poisoned rats. Toxicol Lett 213:142-150.

Ehaideb SN, Decker GT, Smith P, Messimore N, Davis D, Zhang B (2018) Allostatic Compensatory Mechanisms Enable the Mutant KCNT1 Channels to Induce Seizures and Hyperexcitability (2018). . SSRN.

Fenton TA, Haouchine OY, Hallam EB, Smith EM, Jackson KC, Rahbarian D, Canales CP, Adhikari A, Nord AS, Ben-Shalom R, Silverman JL (2024) Hyperexcitability and translational phenotypes in a preclinical mouse model of SYNGAP1-related intellectual disability. Transl Psychiatry 14:405.

Frankel WN, Taylor L, Beyer B, Tempel BL, White HS (2001) Electroconvulsive thresholds of inbred mouse strains. Genomics 74:306-312.

Fusco AF, Pucci LA, Switonski PM, Biswas DD, McCall AL, Kahn AF, Dhindsa JS, Strickland LM, La Spada AR, ElMallah MK (2021) Respiratory dysfunction in a mouse model of spinocerebellar ataxia type 7. Disease models & mechanisms 14.

Gompers AL et al. (2017) Germline Chd8 haploinsufficiency alters brain development in mouse. Nat Neurosci 20:1062-1073.

Hanes AL, Koesters AG, Fong MF, Altimimi HF, Stellwagen D, Wenner P, Engisch KL (2020) Divergent Synaptic Scaling of Miniature EPSCs following Activity Blockade in Dissociated Neuronal Cultures. J Neurosci 40:4090-4102.

Hinckley CA, Zhu Z, Chu JH, Gubbels C, Danker T, Cherry JJ, Whelan CD, Engle SJ, Nguyen V (2023) Functional evaluation of epilepsy-associated KCNT1 variants in multiple cellular systems reveals a predominant gain of function impact on channel properties. Epilepsia 64:2126-2136.

Huie EZ, Yang X, Rioult-Pedotti MS, Tran K, Monsen ER, Hansen K, Erickson MA, Naik M, Yotova AY, Banks WA, Huang YA, Silverman JL, Marshall J (2025) Peptidomimetic inhibitors targeting TrkB/PSD-95 signaling improves cognition and seizure outcomes in an Angelman Syndrome mouse model. Neuropsychopharmacology 50:772-782.

Hussain R, Lim CX, Shaukat Z, Islam A, Caseley EA, Lippiat JD, Rychkov GY, Ricos MG, Dibbens LM (2024) Drosophila expressing mutant human KCNT1 transgenes make an effective tool for targeted drug screening in a whole animal model of KCNT1-epilepsy. Sci Rep 14:3357.

Kuchenbuch M et al. (2019) KCNT1 epilepsy with migrating focal seizures shows a temporal sequence with poor outcome, high mortality and SUDEP. Brain 142:2996-3008.

Lim CX, Ricos MG, Dibbens LM, Heron SE (2016) KCNT1 mutations in seizure disorders: the phenotypic spectrum and functional effects. J Med Genet 53:217-225.

Liu R, Sun L, Wang Y, Wang Q, Wu J (2023) New use for an old drug: quinidine in KCNT1-related epilepsy therapy. Neurol Sci 44:1201-1206.

McManus DQ, Brewer GJ (1997) Culture of neurons from postmortem rat brain. Neurosci Lett 224:193-196.

Miller AR, Hawkins NA, McCollom CE, Kearney JA (2014) Mapping genetic modifiers of survival in a mouse model of Dravet syndrome. Genes Brain Behav 13:163-172.

Mistry AM, Thompson CH, Miller AR, Vanoye CG, George AL, Jr., Kearney JA (2014) Strain- and age-dependent hippocampal neuron sodium currents correlate with epilepsy severity in Dravet syndrome mice. Neurobiol Dis 65:1-11.

Moller RS et al. (2015) Mutations in KCNT1 cause a spectrum of focal epilepsies. Epilepsia 56:e114-120.

Numis AL, Nair U, Datta AN, Sands TT, Oldham MS, Patel A, Li M, Gazina E, Petrou S, Cilio MR (2018) Lack of response to quinidine in KCNT1-related neonatal epilepsy. Epilepsia 59:1889-1898.

Petkova SP, Adhikari A, Berg EL, Fenton TA, Duis J, Silverman JL (2022) Gait as a quantitative translational outcome measure in Angelman syndrome. Autism Res 15:821-833.

Purtell H, Dhamne SC, Gurnani S, Bainbridge E, Modi ME, Lammers SHT, Super CE, Hameed MQ, Johnson EL, 3rd, Sahin M, Rotenberg A (2018) Electrographic spikes are common in wildtype mice. Epilepsy Behav 89:94-98.

Quraishi IH, Mercier MR, McClure H, Couture RL, Schwartz ML, Lukowski R, Ruth P, Kaczmarek LK (2020) Impaired motor skill learning and altered seizure susceptibility in mice with loss or gain of function of the Kcnt1 gene encoding Slack (K(Na)1.1) Na(+)-activated K(+) channels. Sci Rep 10:3213.

Rizzo F, Ambrosino P, Guacci A, Chetta M, Marchese G, Rocco T, Soldovieri MV, Manocchio L, Mosca I, Casara G, Vecchi M, Taglialatela M, Coppola G, Weisz A (2016) Characterization of two de novoKCNT1 mutations in children with malignant migrating partial seizures in infancy. Mol Cell Neurosci 72:54-63.

Rychkov GY, Shaukat Z, Lim CX, Hussain R, Roberts BJ, Bonardi CM, Rubboli G, Meaney BF, Whitney R, Moller RS, Ricos MG, Dibbens LM (2022) Functional Effects of Epilepsy Associated KCNT1 Mutations Suggest Pathogenesis via Aberrant Inhibitory Neuronal Activity. Int J Mol Sci 23.

Seiler S, Rudolf F, Gomes FR, Pavlovic A, Nebel J, Seidenbecher CI, Foo LC (2024) Astrocyte-derived factors regulate CNS myelination. Glia 72:2038-2060.

Shore AN, Li K, Safari M, Qunies AM, Spitznagel BD, Weaver CD, Emmitte KA, Frankel WN, Weston MC (2024) Heterozygous expression of a Kcnt1 gain-of-function variant has differential effects on SST- and PV-expressing cortical GABAergic neurons. bioRxiv.

Shore AN, Colombo S, Tobin WF, Petri S, Cullen ER, Dominguez S, Bostick CD, Beaumont MA, Williams D, Khodagholy D, Yang M, Lutz CM, Peng Y, Gelinas JN, Goldstein DB, Boland MJ, Frankel WN, Weston MC (2020) Reduced GABAergic Neuron Excitability, Altered Synaptic Connectivity, and Seizures in a KCNT1 Gain-of-Function Mouse Model of Childhood Epilepsy. Cell Rep 33:108303.

Silverman JL, Babineau BA, Oliver CF, Karras MN, Crawley JN (2013) Influence of stimulant-induced hyperactivity on social approach in the BTBR mouse model of autism. Neuropharmacology 68:210-222.

Sittig LJ, Carbonetto P, Engel KA, Krauss KS, Barrios-Camacho CM, Palmer AA (2016) Genetic Background Limits Generalizability of Genotype-Phenotype Relationships. Neuron 91:1253-1259.

Spencer MC, Downes JH, Xydas D, Hammond MW, Becerra VM, Warwick K, Whalley BJ, Nasuto SJ (2012) Multiscale evolving complex network model of functional connectivity in neuronal cultures. IEEE Trans Biomed Eng 59:30-34.

Sterlini B, Fruscione F, Baldassari S, Benfenati F, Zara F, Corradi A (2020) Progress of Induced Pluripotent Stem Cell Technologies to Understand Genetic Epilepsy. Int J Mol Sci 21.

Sukoff Rizzo SJ, McTighe S, McKinzie DL (2020) Genetic Background and Sex: Impact on Generalizability of Research Findings in Pharmacology Studies. Handb Exp Pharmacol 257:147-162.

Vanderver A, Simons C, Schmidt JL, Pearl PL, Bloom M, Lavenstein B, Miller D, Grimmond SM, Taft RJ (2014) Identification of a novel de novo p.Phe932Ile KCNT1 mutation in a patient with leukoencephalopathy and severe epilepsy. Pediatr Neurol 50:112-114.

Vertes PE, Alexander-Bloch A, Bullmore ET (2014) Generative models of rich clubs in Hebbian neuronal networks and large-scale human brain networks. Philos Trans R Soc Lond B Biol Sci 369.

Wagenaar DA, Pine J, Potter SM (2006) Searching for plasticity in dissociated cortical cultures on multi-electrode arrays. J Negat Results Biomed 5:16.

Wang R, Teng S, Turanchik M, Zhen F, Peng Y (2025) Tonic-clonic seizures induce hypersomnia and suppress rapid eye movement sleep in mouse models of epilepsy. Sleep Adv 6:zpaf009.

Wu J, Quraishi IH, Zhang Y, Bromwich M, Kaczmarek LK (2024) Disease-causing Slack potassium channel mutations produce opposite effects on excitability of excitatory and inhibitory neurons. Cell Rep 43:113904.

Xu D, Chen S, Yang J, Wang X, Fang Z, Li M (2022) Precision therapy with quinidine of KCNT1-related epileptic disorders: A systematic review. Br J Clin Pharmacol 88:5096-5112.

Yang Y, Frankel WN (2004) Genetic approaches to studying mouse models of human seizure disorders. Adv Exp Med Biol 548:1-11.